journal

J. Am. Ceram. Soc., 80 [5] 1073–78 (1997)

Scaling Analysis for the Axial Displacement and Pressure of Flextensional Transducers

Wan Y. Shih,[†,‡] Wei-Heng Shih,[*,‡] and Ilhan A. Aksay[*,†]

Department of Chemical Engineering and Princeton Materials Institute, Princeton University, Princeton, New Jersey 08544-5263

Department of Materials Engineering, Drexel University, Philadelphia, Pennsylvania 19104-2875

We have examined the axial displacement, Δh, and maximum axial pressure, P_{max}, of flextensional transducers such as the moonies and the rainbows with both scaling and mechanical analyses. For a constant electric field E across the transducer, $\Delta h/t \propto E/t^2$ where t is the thickness of the rainbow or the thickness of the metal end cap of the moonie and $\Delta h/t$, the relative axial displacement. Thus, for a constant voltage V across the transducer, $\Delta h/t \propto V/t^3$. As for the maximum pressure, $P_{max} \propto t^2$ for the rainbows and $P_{max} \propto wt$ for the moonies where t is the thickness of the rainbow or the thickness of the metal end cap of the moonie and w the thickness of the piezoelectric disk of the moonie. These predictions agree well with the experimental results found in the rainbows and the moonies. Our analysis showed that although the rainbows and the moonies differ in design and processing, the underlying physics for the enhancement in the axial displacement are essentially the same: The nonuniform distribution of d_{31} through the thickness of the transducer causes the transducer to arch or flatten with an applied electrical field, which leads to the enhancement in the axial displacement. The only difference is that, for the transducer to arch, the applied field is in the opposite direction to the polarization in the rainbows but in the same direction as the polarization in the moonies.

I. Introduction

RECENTLY, several new actuators with improved properties have been developed. One is the ceramic–metal composite actuator called the moonie developed by Sugawara *et al.*[1] Another is the reduced and internally biased oxide wafer abbreviated as the rainbow developed by Haertling.[2] Both the moonies and the rainbows are flextensional transducers. These two actuators are conceptually similar in that they both (i) contain a shell structure and (ii) attain large axial displacement at the apex of the shell through induced bending stresses. The moonie actuator can produce displacements as high as 20 μm at a stress of 0.5 MPa. The rainbow has been shown to produce displacements up to 1 mm. Although the displacement produced by a rainbow actuator can be large, the sustaining stress is relatively moderate. The moonie is composed of a piezoelectric disk, e.g., lead-zirconate-titanate (PZT) with a hollow metal end cap at the top as schematically shown in Fig. 1(a). An axial displacement of the metal end cap is generated when an electric field is applied across the thickness of the piezoelectric disk. By varying the thickness of the metal end cap and/or the diameter of the piezoelectric disk, axial displacements as high as 8% of the thickness of the metal end cap have been achieved at the center of the metal end cap.[3] The rainbow is an oxide piezoelectric disk such as lead-lanthanum-zirconate-titanate (PLZT) with one of the two faces of the disk reduced. The cross-section view of a rainbow is schematically shown in Fig. 1(b).[2] An axial displacement is generated when an electric field is applied across the thickness of the rainbow. By varying the thickness and/or the diameter of the disk, axial displacements as high as 600% have been achieved.[2] The axial displacements of both the moonies and the rainbows are orders of magnitude larger than those of the traditional direct extensional devices. In addition, they exhibit strong size dependence.

In view of the large axial displacements displayed by the two new actuators, it is of fundamental as well as practical importance to understand the underlying mechanism for the enhancement. The objective of this paper is to analyze and compare the axial displacement and maximum axial pressure of both the rainbows and the moonies. Our approach is to use scaling as well as mechanical analyses. Although finite-element analyses have been performed for the moonies for their hydrophone application,[4] so far there has been no theory that analyzes and compares the two devices as actuators. Our analyses show that although the moonies and the rainbows differ in design and processing, the underlying physics for the enhancement in the axial displacement are essentially the same. In both actuators, it is the nonuniform distribution of the piezoelectric coefficient d_{31} in the axial direction that gives rise to the strong size dependence and hence the enhancement in the axial displacement. Our scaling and mechanical analyses agree well with the experiments.

II. Rainbows

(1) Displacement

(A) Mechanical Analysis: One of the two faces of the piezoelectric disk of the rainbow transducer is reduced as schematically shown in Fig. 1(b). As a result, the piezoelectric coefficient d_{31} in the reduced layer is largely diminished. Thus, one may simplify the rainbow transducer as a piezoelectric–nonpiezoelectric composite strip with the nonpiezoelectric part representing the reduced layer. A schematic piezoelectric–nonpiezoelectric strip is shown in Fig. 2 where t_p and t_{np} are the

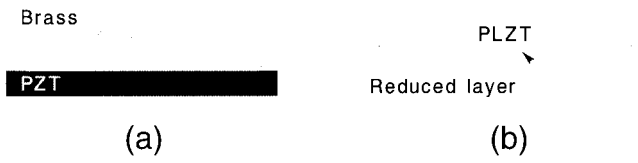

Fig. 1. Schematic of (a) the moonie and (b) the rainbow.

Walter A. Schulze—contributing editor

Manuscript No. 191939. Received March 5, 1996; approved August 21, 1996.
Supported by the Army Research Office Multidisciplinary University Research Initiative (ARO/MURI) under Grant No. DAAH04-95-1-0102.
*Member, American Ceramic Society.
†Princeton University.
‡Drexel University.

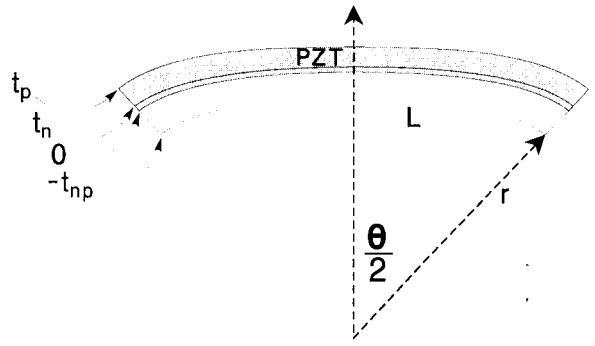

Fig. 2. Schematic of a piezoelectric–nonpiezoelectric strip where t_p and t_{np} are the thickness of the piezoelectric strip and that of the nonpiezoelectric strip, respectively. The boundary between the piezoelectric and nonpiezoelectric strips is chosen as the origin, and t_n denotes the position of the neutral plane.

thickness of the piezoelectric strip and that of the nonpiezoelectric strip, respectively. With the boundary between the piezoelectric and nonpiezoelectric strips as the origin, t_n denotes the position of the neutral plane. The piezoelectric coefficient d_{31} is nonuniform in such a transducer. It has a stepwise distribution: $d_{31} \neq 0$ in the piezoelectric layer and $d_{31} = 0$ in the nonpiezoelectric layer as schematically shown in Fig. 3. With the assumption that the thickness of the transducer is much smaller than the radius of curvature of the transducer, the strain ε at an axial position z within the transducer is then[5]

$$\varepsilon = \left(\frac{z - t_n}{r}\right) + c \tag{1}$$

where t_n is the radial position of the neutral axis, r the radius of curvature of the inner surface of the transducer, and c the constrained in-plane strain due to, for example, the piezoelectric coefficient mismatch and/or the thermal expansion coefficient mismatch between the two layers. When an external electric field E is applied across the thickness of the transducer, the stress in the piezoelectric layer becomes $\sigma_p = E_p[c - \alpha_p\Delta T - d_{31}E]$ while that in the nonpiezoelectric region is $\sigma_{np} = E_{np}[c - \alpha_{np}\Delta T]$. ΔT is the temperature difference between room temperature and the processing (reduction) temperature, and E_p, α_p, and d_{31} are, respectively, Young's modulus, the thermal expansion coefficient, and the piezoelectric coefficient of the piezoelectric layer. E_{np} and α_{np} are, respectively, Young's modulus and the thermal expansion coefficient of the nonpiezoelectric layer. The stress distribution within the transducer must obey the following three boundary conditions:[5]
(i) The sum of the bending stresses equals zero, i.e.,

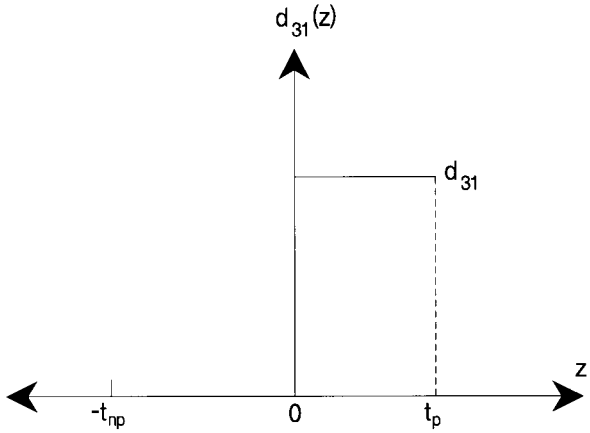

Fig. 3. Schematic of the piezoelectric coefficient d_{31} as a function of the axial position across the thickness of the transducer: $d_{31} \neq 0$ in the piezoelectric layer and $d_{31} = 0$ in the nonpiezoelectric layer.

$$\int_{-t_{np}}^{0} E_{np}\left[\frac{z - t_n}{r}\right]dz + \int_{0}^{t_p} E_p\left[\frac{z - t_n}{r}\right]dz = 0 \tag{2}$$

(ii) The sum of the lateral stresses equals zero, i.e.,

$$\int_{-t_{np}}^{0} E_{np}(c - \alpha_{np}\Delta T)dz + \int_{0}^{t_p} E_p[c - \alpha_p\Delta T - d_{31}E]dz = 0 \tag{3}$$

and (iii) the sum of the bending moments with respect to the neutral axis equals zero, i.e.,

$$\int_{-t_{np}}^{0} E_{np}\left[c + \alpha_{np}\Delta T + \frac{z - t_n}{r}\right](z - t_n)dz + \int_{0}^{t_p} E_p\left[c - \alpha_p\Delta T - d_{31}E + \frac{z - t_n}{r}\right](z - t_n)dz = 0 \tag{4}$$

In Eqs. (2)–(4), the axial coordinate is chosen such that the origin is at the boundary between the piezoelectric and nonpiezoelectric layers. The three boundary conditions, Eqs. (2)–(4), yield the following solutions[5] for the three unknowns, t_n, c, and r:

$$t_n = \frac{E_p t_p - E_{np} t_{np}}{2(E_p t_p + E_{np} t_{np})} \tag{5}$$

$$c = \frac{E_p t_p(\alpha_p\Delta T + d_{31}E) + E_{np} t_{np}\alpha_{np}\Delta T}{E_p t_p + E_{np} t_{np}} \tag{6}$$

$$\frac{1}{r} = \frac{6E_p E_{np} t_p t_{np}(t_p + t_{np})[d_{31}E + (\alpha_p - \alpha_{np})\Delta T]}{E_{np}^2 t_{np}^4 + E_p^2 t_p^4 + 2E_{np}E_p t_{np} t_p(2t_p^2 + 2t_{np}^2 + 3t_p t_{np})} \tag{7}$$

Defining θ as the angle that encompasses the width of the transducer, i.e., $\theta = L/r$ where L and r are, respectively, the lateral width and the curvature of the inner surface of the transducer. The height h of the transducer in the axial direction is related to r and θ as

$$h = t + r\left(1 - \cos\frac{\theta}{2}\right) \cong t + r\frac{\theta^2}{8} = t + \frac{1}{8}\frac{L^2}{r} \tag{8}$$

where t is the total thickness of the transducer. Substituting Eq. (7) into Eq. (8), we obtain

$$h = t + \frac{L^2}{8}\frac{6E_p E_{np} t_p t_{np}(t_p + t_{np})[d_{31}E + (\alpha_p - \alpha_{np})\Delta T]}{E_{np}^2 t_{np}^4 + E_p^2 t_p^4 + 2E_{np}E_p t_{np} t_p(2t_p^2 + 2t_{np}^2 + 3t_p t_{np})} \tag{9}$$

With t_{np} rewritten as $t_{np} = t - t_p$, h becomes

$$h = t + \frac{L^2}{8}\frac{6E_p E_{np} t_p(t - t_p)t[d_{31}E + (\alpha_p - \alpha_{np})\Delta T]}{E_{np}^2(t - t_p)^4 + E_p^2 t_p^4 + 2E_{np}E_p(t - t_p^2)t_p[2t_p^2 + 2(t - t_p)^2 + 3t_p(t - t_p)]} \tag{10}$$

From Eq. (10), for a given t, h varies by changing t_p. The maximum of h is obtained when

$$\left.\frac{\partial h}{\partial t_p}\right|_{t_p = t_{p,max}} = 0 \tag{11}$$

Equation (11) leads to $E_p t_{p,max}^2 = E_{np}(t - t_{p,max})^2$, i.e.,

$$t_{p,max} = \frac{t}{1 + (E_p/E_{np})^{1/2}} \tag{12}$$

The maximum height, h_{max}, is obtained when $t_p = t_{p,max}$ and

$$h_{max} = t + \frac{3L^2}{16t}[d_{31}E + (\alpha_p - \alpha_{np})\Delta T] \tag{13}$$

With $h_0 = t + \frac{3L^2}{16t}(\alpha_p - \alpha_{np})\Delta T$, the maximum displacement due to the piezoelectric effect, $\Delta h_{max} \equiv h_{max} - h_0$, is

$$\Delta h_{max} = \frac{3L^2 d_{31} E}{16t} \tag{14}$$

Therefore, when the applied electric field E is constant across the thickness of the transducer, the relative displacement, $\Delta h_{max}/t$ is inversely proportional to t^2 as

$$\frac{\Delta h_{max}}{t} = \frac{3L^2 d_{31} E}{16t^2} \propto \frac{E}{t^2} \tag{15}$$

Alternatively, if the voltage V applied across the thickness of the transducer is constant, the relative displacement, $\Delta h_{max}/t$ is inversely proportional to t^3, i.e.,

$$\frac{\Delta h_{max}}{t} = \frac{3L^2 d_{31} V}{16t^3} \propto \frac{V}{t^3} \tag{16}$$

(B) Scaling Analysis: The scaling relationships Eqs. (15) and (16) between the axial displacement, Δh, and the thickness of the transducer, t, is not restricted to the piezoelectric–nonpiezoelectric-strip model as depicted in Fig. 2 where d_{31} has a stepwise distribution in the axial direction (see Fig. 3). In the following, we show that the scaling relationships of Eqs. (15) and (16) still hold when the variation of d_{31} in the axial position takes on another form, e.g., d_{31} varies linearly with the axial position. The gradient in d_{31} with respect to the axial direction gives rise to variation of the lateral strain along the axial direction when an electric field is applied across the thickness of the transducer. As the lateral strain varies along the axial direction, the transducer arches as shown schematically in Fig. 4. Let L_1 and L_2 denote, respectively, the lateral widths of the outer and inner surfaces of the transducer. As can be seen from Fig. 4,

$$\Delta L = L_1 - L_2 = (r_1 - r_2)\theta = t\theta \tag{17}$$

where r_1 and r_2 denote the radii of curvature of the outer and inner surfaces, respectively, and θ the angle encompassing the width of the transducer. The difference in the lateral widths between the outer and inner surfaces can arise from both the gradient in the thermal expansion coefficient and that in the piezoelectric coefficient in the transducer, i.e.,

$$\Delta L = \Delta L_0 + \Delta L_{pe} \tag{18}$$

where ΔL_0 is the part due to the gradient in the thermal strain and ΔL_{pe} the part due to the gradient in the piezoelectric strain. ΔL_0 is related to the temperature difference between the application and the heat-treatment temperatures:

$$\Delta L_0 = (\alpha_1 - \alpha_2)\Delta T L \tag{19}$$

where α_1 and α_2 are the thermal expansion coefficients on the outer and inner surfaces, respectively, and L the width of the transducer at the heat-treatment temperature. Due to the gradient in the piezoelectric coefficient, the lateral piezoelectric strain varies in the axial direction when an electric field E is applied across the thickness of the transducer. The resultant length difference between the outer and inner surfaces is

$$\Delta L_{pe} = E\int_0^t \frac{d d_{31}(z)}{dz} L(z)\, dz \tag{20}$$

where z denotes the coordinate along the axial direction. For a linear variation of d_{31} with respect to z, $dd_{31}/dz = \Delta d_{31}/t$, where $\Delta d_{31} = d_{31}(z = t) - d_{31}(z = 0)$. Therefore, for $\Delta L \ll L_1, L_2 \approx L$,

$$\theta = \frac{\Delta L}{t} \approx \frac{\Delta L_0 + (\Delta d_{31} E)L}{t} \tag{21}$$

Meanwhile, the height of the transducer is

$$h = r_1 - r_2 \cos(\theta/2) \approx t + \frac{1}{8} r_2 \theta^2 \approx t + \frac{1}{8} L\theta$$
$$= t + \frac{\Delta L_0 L}{8t} + \frac{(\Delta d_{31} E)L^2}{8t} \tag{22}$$

Denoting

$$h_0 = t + \frac{\Delta L_0 L}{8t} \tag{23}$$

as the height in the absence of the electric field, the displacement due to the applied electric field is then

$$\Delta h = h - h_0 = \frac{(\Delta d_{31} E)}{8}\frac{L^2}{t} \tag{24}$$

i.e.,

$$\Delta h \sim \frac{1}{8}\Delta d_{31} L^2 \frac{E}{t} \tag{25}$$

The relative displacement $\Delta h/t$ is, therefore,

$$\frac{\Delta h}{t} \sim \frac{1}{8}\Delta d_{31} L^2 \frac{E}{t^2} \tag{26}$$

When the applied electric field is constant across the thickness of the transducer, the relative displacement is inversely proportional to t^2. When the voltage V across the thickness is constant, the relative displacement is then inversely proportional to t^3 as

$$\frac{\Delta h}{t} \sim \frac{1}{8}\Delta d_{31} L^2 \frac{V}{t^3} \tag{27}$$

If $d_{31}(z = t) = d_{31}$ and $d_{31}(z = 0) = 0$, then Eqs. (26) and (27) become

$$\frac{\Delta h}{t} \sim \frac{1}{8} d_{31} L^2 \frac{E}{t^2} \tag{28}$$

and

$$\frac{\Delta h}{t} \sim \frac{1}{8} d_{31} L^2 \frac{V}{t^3} \tag{29}$$

respectively. Note that the scaling relationships Eqs. (28) and (29) obtained by the scaling analysis are essentially the same as those obtained by the mechanical analysis, Eqs. (15) and (16), except that the preconstant is 1/8 in Eqs. (28) and (29) and 3/16 in Eqs. (15) and (16). The difference in the numerical values of the preconstants results from the different forms of the variation of d_{31} along the axial direction. For the mechanical analysis, the variation of d_{31} takes on a stepwise form, whereas for the scaling analysis d_{31} varies linearly with z.

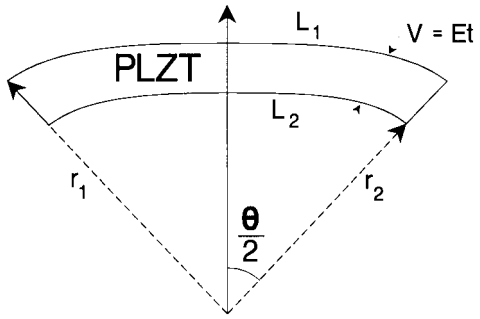

Fig. 4. Schematic of the rainbow.

(2) Axial Pressure

The scaling relationship of the maximum pressure P_{max} of the transducer with respect to width, L, and thickness, t, can be

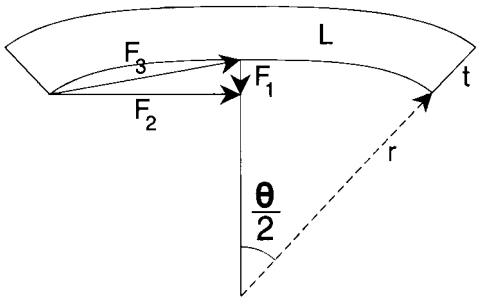

Fig. 5. Schematic of the forces acting on the rainbow when an axial pressure P is applied.

obtained as follows. Let P denote the applied pressure in the axial direction. Figure 5 is a schematic of all the forces exerted on a rainbow when an axial pressure P is applied on the rainbow. The total applied force in the axial direction is therefore

$$F_1 = P\pi x^2 \tag{30}$$

where x is the radius of the horizontal projection of the dome. Denoting the stress in the lateral direction as T_θ, the total force in the lateral direction is therefore

$$F_3 = T_\theta 2\pi x t \tag{31}$$

The sum of the axial components of all forces equals zero, implying that

$$\frac{F_1}{F_3} = \sin(\theta/2) \tag{32}$$

For small θ, Eq. (32) yields

$$P = T_\theta t \frac{1}{x}\frac{\theta}{2} \tag{33}$$

With $x \sim L$, $\theta \sim t/L$,

$$P \sim \frac{1}{2} T_\theta \frac{t^2}{L^2} \tag{34}$$

Thus, the maximum axial pressure P_{max} that the transducer can withstand becomes

$$P_{max} \sim T_{\theta,max}\frac{t^2}{L^2} \tag{35}$$

where $T_{\theta,max}$ is the maximum stress in the lateral direction that the material can withstand. As $T_{\theta,max}$ is a material constant,

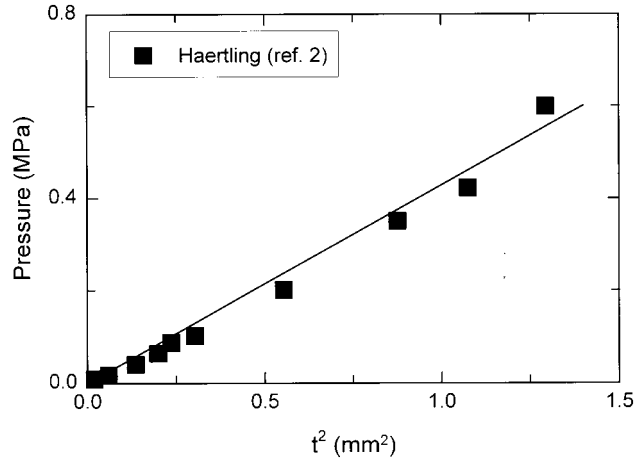

Fig. 7. P_{max} versus t^2 for rainbows where P_{max} is the maximum axial pressure that the rainbow can withstand.

$$P_{max} \sim \frac{t^2}{L^2} \tag{36}$$

(3) Comparison with Experiments

In Haertling's experiments, the displacements of the rainbows of various thickness were measured with a constant voltage V across the thickness of the rainbows. According to the result of both the mechanical analysis depicted in Eq. (16) and of the scaling analysis depicted in Eqs. (27) and (29), the relative displacement of the rainbow should be inversely proportional to t^3 with a constant voltage V across the thickness of the transducer. In Fig. 6(a), we plot the relative displacement $\Delta h/t$ versus t^{-3}. The data points were taken from Haertling's experiments,[2] and the straight line is to guide the eye. Figure 6(b) is a magnification of the rectangular region at the lower left corner of Fig. 6(a). All data points fall on a straight line over the entire thickness range, indicating that the relative displacement $\Delta h/t$ is indeed inversely proportional to t^3 with a constant voltage V across the thickness as predicted by both the mechanical analysis (Eq. (16)) and the scaling analysis (Eqs. (27) and (29)). The maximum pressure P_{max} versus t^2 for rainbows of various thickness is plotted in Fig. 7. Again, the data points were taken from the experiments of Haertling,[2] and the straight line is to guide the eye. All the data points fall on the straight line, indicating that P_{max} is indeed proportional to t^2 as predicted by the scaling analysis (Eq. (36)).

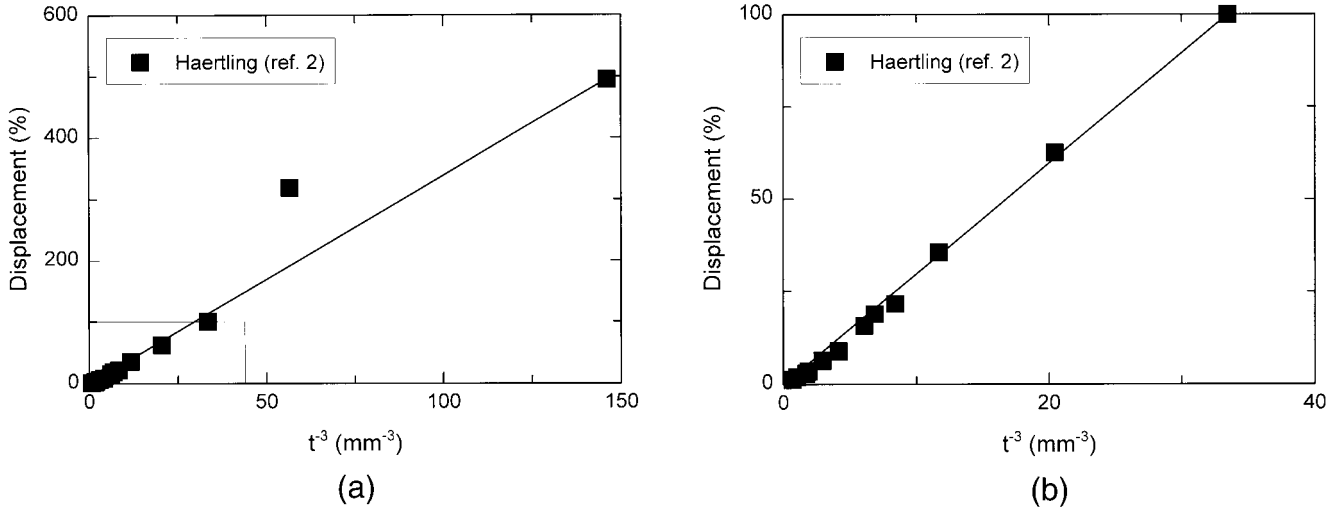

Fig. 6. (a) $\Delta h/t$ versus t^{-3} for rainbows with a constant voltage V across the thickness t of the rainbow where $\Delta h/t$ denotes the relative displacement. The data points were taken from the experiments of Haertling.[2] (b) Magnification of the rectangular region at the lower left corner of (a).

Besides the variation of the displacement and the maximum pressure with respect to the total thickness discussed above, Moon and Haertling[6] have also varied the ratio t_{np}/t for rainbows of a given total thickness t and measured the corresponding axial displacements. They showed that a maximum in the axial displacement exists at around $t_{np}/t \cong 0.35$ for PLZT with a composition 1/53/47 for La/Zr/Ti.[6] This result qualitatively agrees with the prediction of our mechanical analysis that, for a given t, the axial displacement is maximized at a particular t_p/t (see Eq. (13)). Using the values of Young's moduli, $E_p = 6.287 \times 10^{10}$ N/m^2 and $E_{np} = 4.455 \times 10^{10}$ N/m^2 measured by Moon and Haertling,[6] Eq. (13) predicts that the maximum displacement occurs at about $t_{np}/t \cong 0.54$. The reason for the numerical discrepancy between the prediction of Eq. (13) and the experimental result of Moon and Haertling[6] is unclear at the moment. The assumption of the theory that d_{31} is constant within each layer probably oversimplifies the distribution of d_{31} within the transducer. The rainbow transducers were made by reduction on one side. It is likely that the boundary between the piezoelectric layer and the nonpiezoelectric layer is not as clear cut as a step function. More discussion on this is given in the concluding remarks. Meanwhile, it is also known that the rainbow transducers can exhibit more than one radius of curvature, which is not considered in the present theory.

III. Moonies

(1) Scaling Analysis

(A) Axial Displacement: The schematic of a moonie is shown in Fig. 8(a). Let L denote the diameter of the piezoelectric disk, L_m the length of the metal end cap, t the initial height of the metal end cap. Upon the application of an electric field across the thickness of the piezoelectric disk, the piezoelectric disk exhibits a displacement ΔL in the lateral direction with

$$\Delta L = d_{31} E L \tag{37}$$

where d_{31} is the piezoelectric coefficient of the piezoelectric disk. Let us assume a perfect bonding between the metal end cap and the piezoelectric disk. Hence, the metal end cap should have the same lateral displacement, ΔL, as the piezoelectric disk when an electric field is applied across the piezoelectric disk. Let Δh denote the axial displacement of the metal end cap after the electric field is applied. The length of the metal end cap before and after the application of an electric field can be approximated as $L_m \cong 2\sqrt{(L/2)^2 + t^2}$ and $L'_m \cong 2\sqrt{[(L + \Delta L)/2]^2 + (t + \Delta h)^2}$, respectively. Since the piezoelectric coefficient of the metal end cap is zero, $L_m = L'_m$. To the first order in ΔL and Δh, the requirement that $L_m = L'_m$ leads to

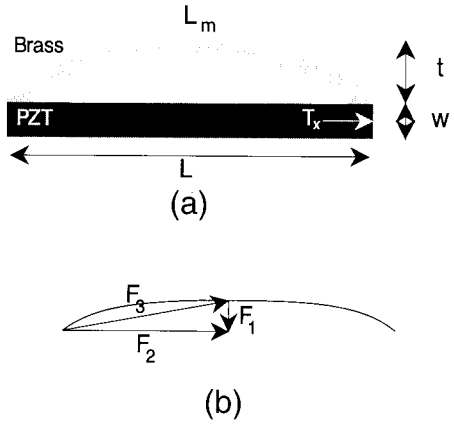

Fig. 8. (a) Schematic of the moonie. (b) Schematic of the forces acting on the moonie when an axial pressure P is applied on the metal cap.

$$\frac{L}{2}\Delta L = -t\Delta h \tag{38}$$

From Eq. (38) one can see that if the piezoelectric disk contracts ($\Delta L < 0$), the metal cap arches. Conversely, if the piezoelectric disk extends ($\Delta L > 0$), the metal end cap flattens. The height of the metal end cap changes as the width of the metal end cap varies. Combining Eqs. (37) and (38), the axial displacement Δh and the relative displacement $\Delta h/t$ at a constant E can be written as

$$\Delta h = -\frac{d_{31} E L^2}{2t} \tag{39}$$

and

$$\frac{\Delta h}{t} = -\frac{d_{31} E L^2}{2t^2} \tag{40}$$

respectively. With a constant E, the relative displacement $\Delta h/t$ is proportional to L^2 and inversely proportional to t^2. The result shown in Eq. (40) is very similar to that of the rainbows shown in Eq. (28) only that, for the rainbows, t is the thickness of the rainbow, whereas for the moonies t is the thickness of the metal end cap. Although the rainbows and the moonies share the same scaling behavior of the displacement, the sign of the displacement of the rainbow is actually opposite to that of the moonie with the same applied field. This can be seen from the difference in the sign in Eq. (28) and Eq. (40). Let us define the electric field E to be positive when it is parallel to the polarization. Eqs. (28) and (40) show that the proportional constant of the axial displacement of the rainbows with respect to E is proportional to $+d_{31}$, whereas that of the moonie is proportional to $-d_{31}$. With d_{31} being negative for PZT and PLZT, it follows that the rainbows would flatten ($\Delta h < 0$) but the moonies would arch ($\Delta h > 0$) when E is positive. Conversely, the rainbows would arch and the moonies would flatten when the sign of the field is reversed.

(B) Maximum Pressure: Figure 8(b) schematically shows the forces acting on the moonie when an axial pressure is applied on the metal cap. The axial pressure P on the metal cap creates a net force, F_1, in the axial direction as

$$F_1 = P\frac{\pi L^2}{4} \tag{41}$$

The axial pressure P on the metal cap creates a lateral stress T_x in the piezoelectric disk. The net lateral force in the piezoelectric disk is then

$$F_2 = T_x(\pi L)w \tag{42}$$

where w is the thickness of the piezoelectric disk. As the ceramic piezoelectric disk is much more brittle than the metal cap, the maximum pressure that the actuator can withstand is limited by the maximum lateral stress that the piezoelectric disk can withstand. As can be seen from Fig. 8(b), the forces F_1 and F_2 must satisfy the following relation:

$$\frac{F_1}{F_2} = \frac{h}{L/2} \tag{43}$$

where h is the height of the metal cap measured from the metal–PZT boundary under pressure, P. Thus, the axial pressure of the transducer, P, is related to the lateral stress in the piezoelectric disk, T_x, as

$$P = T_x\frac{(2wh)}{L^2} \tag{44}$$

Therefore, the maximum axial pressure, P_{max}, that a moonie can withstand is

$$P_{max} = T_{x,max}\frac{(2wh)}{L^2} \tag{45}$$

where $T_{x,max}$ is the maximum stress that the piezoelectric disk can withstand, which is a material constant. With $h \approx t$,

$$P_{max} \approx T_{x,max} \frac{(2wt)}{L^2} \tag{46}$$

For the rainbows, P_{max} is proportional to t^2, whereas for the moonies, P_{max} is proportional to the product of t and w.

(2) Comparison with Experiments

The axial displacements of moonies were measured with a constant electric field E applied across the thickness of the piezoelectric disk. Therefore, Eq. (40) should apply. The relative displacement $\Delta h/t$ should be inversely proportional to t^2 when the thickness of the metal end cap, t, is varied. We plot the relative displacement $\Delta h/t$ versus t^{-2} for the moonies in Fig. 9. The data points were taken from the experiments of Onitsuka *et al*.[3] The straight line is to guide the eye. All the data points fall on the straight line, indicating that $\Delta h/t$ is indeed inversely proportional to t^2 for a constant E across the thickness of the piezoelectric disk.

IV. Concluding Remarks

The underlying principle for the enhancement in the axial displacement for both moonies and rainbows is very similar: by joining a piezoelectric strip with a nonpiezoelectric strip, the piezoelectric strip responds to the axial electric field, while the nonpiezoelectric strip does not, and thus the device arches or flattens. The scaling analysis as well as the mechanical analysis for a rainbow shows that the relative axial displacement follows $\Delta h/t \sim d_{31}L^2E/t^2$ (or $\Delta h/t \sim d_{31}L^2V/t^3$) for a constant electric field E (a constant voltage V) across the thickness t of the rainbow. The $\Delta h/t \sim V/t^3$ relationship is in good agreement with the experiments of Haertling.[2] The scaling results also predict that the displacement would be larger for rainbows with larger diameters. The scaling analysis shows that the maximum axial pressure that the rainbow can withstand is $P_{max} \sim t^2/L^2$. The $P_{max} \sim t^2$ scaling relationship is also in good agreement with the experiments of Haertling.[2] For the moonies, the relative displacement follows $\Delta h/t \sim -d_{31}L^2E/t^2$ at a constant E across the thickness of the piezoelectric disk, where t and L are the thickness of the metal end cap and the diameter of the piezoelectric disk, respectively. The maximum axial pressure that the moonies can withstand is $P_{max} \sim wt/L^2$, where w is the thickness of the piezoelectric disk. The $\Delta h/t \sim E/t^2$ scaling relationship is in good agreement with the existing experiments of Onitsuka *et al*.[3]

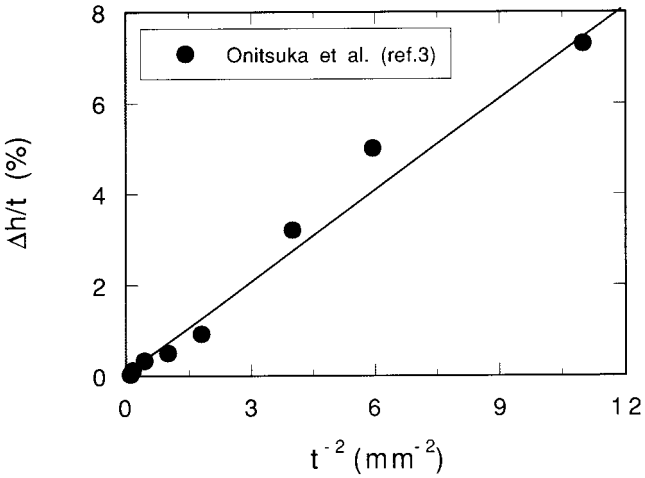

Fig. 9. $\Delta h/t$ versus t^{-2} for moonies where $\Delta h/t$ denotes the relative axial displacement. The data points were taken from the experiments of Onitsuka *et al*.[3]

There is a difference between the rainbows and the moonies regarding the direction of the displacement with respect to the direction of the electric field, as can be seen from Eqs. (28) and (40). In order for the transducer to arch, the applied field is in the opposite direction to the polarization in the rainbows but in the same direction as the polarization in the moonies. This is due to the fact that in the moonies the metal is in the outer part of the arch, whereas in the rainbows the metal (reduced layer) is in the inner part of the arch. Other than that, the underlying physics that govern the enhancement of the axial displacement are the same for both the rainbows and the moonies. In principle, both the moonies and the rainbows can achieve very high axial displacements if an appropriate ratio, L/t, is chosen where L is the width of the device for both the moonies and the rainbows and t is the thickness of the rainbow or the thickness of the metal end cap of the moonies. The difference in the axial displacements of the existing rainbows and moonies is mainly due to the difference in the L/t ratio. So far, the rainbows have achieved higher axial displacements than the moonies, mainly because the rainbows have had the higher L/t ratios. Similarly, appropriate axial pressures can be achieved with an appropriate t/L for both the rainbows and the moonies.

Finally, the scaling analysis is only qualitative. It is impossible to perform quantitative comparisons with experiments by this means. The merit of the scaling analysis is its ease to unveil the underlying physics. On the other hand, the mechanical analysis can be quantitatively compared with the experiments. A few points must be considered in order for detailed comparisons with the experiments to be made. First, in the mechanical analysis, the axial distribution of d_{31} is assumed to be stepwise. It is known that most interfaces exhibit a hyperbolic tangent profile. In particular, the interface between the piezoelectric layer and the reduction layer is related to diffusion. It is likely that the axial variation of d_{31} has a more complex form than a step function. A reasonable distribution of d_{31} may be

$$d_{31}(z) = \frac{1}{2}d_{31}\left[1 + \tanh\left(\frac{z}{\delta}\right)\right] \tag{47}$$

where δ is the half-width of the interface. By considering a finite width for the interface, the prediction for the ratio t_{np}/t at which the maximum axial displacement occurs will be substantially modified. Meanwhile, the present mechanical analysis is essentially two-dimensional; i.e., it only considered the axial and the lateral directions. The effect of the third dimension must be considered. These considerations are important for detailed quantitative comparisons with the experiments.

Acknowledgment: We thank D. M. Dabbs for his assistance.

References

[1]Y. Sugawara, K. Onitsuka, S. Yoshikawa, Q. C. Xu, R. E. Newnham, and K. Uchino, "Metal–Ceramic Composite Actuators," *J. Am. Ceram. Soc.*, **75** [4] 996–98 (1992).

[2]G. H. Haertling, "Rainbow Ceramics: A New Type of Ultra-High-Displacement Actuators," *Am. Ceram. Soc. Bull.*, **73** [1] 93–96 (1994).

[3]K. Onitsuka, A. Dogan, Q. Xu, S. Yoshikawa, and R. E. Newnham, "Design Optimization for Metal–Ceramic Composite Actuators: Moonie," *Ferroelectrics*, **156**, 37–42 (1994).

[4]Q. C. Xu, S. Yoshikawa, J. R. Belsick, and R. E. Newnham, "Piezoelectric Composites with High Sensitivity and High Capacitance for Use at High Pressures," *IEEE Trans. Ultrason. Ferroelectr. Freq. Control*, **38** [6] 634–39 (1991).

[5]C. H. Hsueh and A. G. Evans, "Residual Stress in Metal/Ceramic Bonded Strips," *J. Am. Ceram. Soc.*, **68** [5] 241–48 (1985).

[6]Y. Moon and G. H. Haertling, "The Processing Effects on the Performance of PLZT Rainbow Ceramics"; presented at the 97th annual meeting of the American Ceramic Society, April, 1995 (Paper No. EP-18-95). □